Acta Crystallographica Section B
Structural Science
ISSN 0108-7681

Structure determination of $Mg_3(OH)_5Cl{\cdot}4H_2O$ (F5 phase) from laboratory powder diffraction data and its impact on the analysis of problematic magnesia floors

Kunihisa Sugimoto,[a] Robert E. Dinnebier[a]* and Thomas Schlecht[b]

[a]Max-Planck Institute for Solid State Research, Heisenbergstrasse 1, D-70569 Stuttgart, Germany, and [b]Wilhelm-Röntgen-Straße 25/1, D-73760 Ostfildern, Germany

Correspondence e-mail: r.dinnebier@fkf.mpg.de

Received 7 May 2007
Accepted 22 September 2007

The crystal structure with the idealized formula $Mg_3(OH)_5Cl{\cdot}4H_2O$, the so-called F5 phase according to $5Mg(OH)_2{\cdot}MgCl_2{\cdot}8H_2O$ in the system $MgCl_2$–MgO–H_2O, has been solved *ab initio* from high-quality laboratory powder diffraction data at room temperature. The F5 phase is structurally related to $3Mg(OH)_2{\cdot}MgCl_2{\cdot}8H_2O$ (F3 form). The F5 phase consists of infinite triple chains with one $Mg(OH)_6$ and two $Mg(OH)_4(OH_2)_2$ octahedra as building units intercalated by chlorides, which are partly substituted by disordered hydroxides in the real structure. The F5 phase is of technological importance as the most important binder phase in Sorel cements. Knowledge of the crystal structure enables the full quantitative phase analysis of magnesia cements for the first time, which turns out to be very helpful in the search for possible causes of broken or bleached magnesia floors. Two real-life examples are given.

1. Introduction

In 1867 the French physicist Stanislas Sorel found out that high-quality cement is formed by mixing magnesium oxide with an aqueous solution of magnesium chloride (Sorel, 1867). These so-called Sorel cements have a remarkable capacity to bond with and contain other organic and inorganic materials. Many properties of this magnesia cement are superior to those of Portland cement, namely the high fire resistance, low thermal conductivity, high resistance to abrasion *etc*. The main application for these cements are grindstones, tiles, artificial stone (cast stone), cast floors and even artificial ivory (*e.g.* for billiard balls). On the down side, magnesia cements show a poor resistance to prolonged exposure to water, making them unsuitable for construction applications or for toxic and hazardous waste immobilization.

During the binding process ternary magnesium oxychloride phases are formed, which are of key importance for the properties of the cement. A detailed knowledge of the ternary phase diagram MgO–$MgCl_2$–H_2O is therefore necessary to understand the properties of these cements and to perform any type of qualitative or quantitative phase analysis. So far, four magnesium oxychloride phases are known in this phase diagram: $2Mg(OH)_2{\cdot}MgCl_2{\cdot}5H_2O$ (F2 form), $3Mg(OH)_2{\cdot}MgCl_2{\cdot}8H_2O$ (F3 form), $5Mg(OH)_2{\cdot}MgCl_2{\cdot}8H_2O$ (F5 form) and $9Mg(OH)_2{\cdot}MgCl_2{\cdot}6H_2O$ (F9 form). The only two phases found at a temperature below 373 K and thus occurring in Sorel cements are the F3 and the F5 phases (Bilinski *et al.*, 1984). The crystal structure of the F3 phase was solved from powder diffraction data (de Wolff & Walter-Lévy, 1953), while that of the F5 phase was unknown until now. Depending on the production and the setting process, the aging and envir-

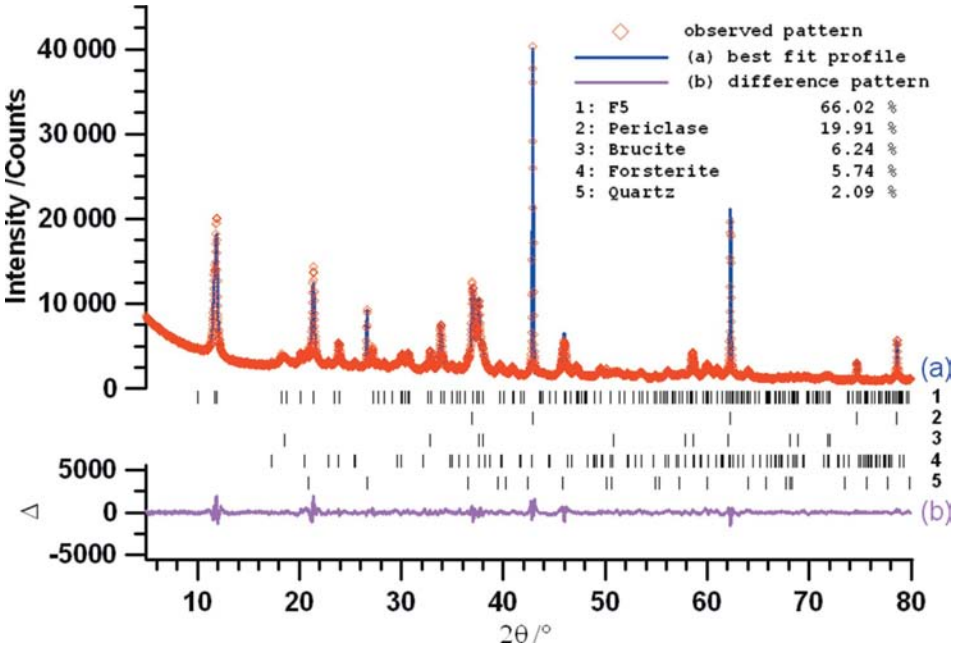

Figure 1
Scattered X-ray intensity for $Mg_3(OH)_5Cl{\cdot}4H_2O$ (F5 phase) at T = 295 K as a function of the diffraction angle 2θ. Shown are the observed pattern (diamonds), the best Rietveld-fit profile [line (*a*)], the difference curve between observed and calculated profile [line (*b*)], and the reflection markers (vertical bars). The additional phases included in the Rietveld refinement are periclase, brucite, forsterite and quartz. Thus, the F5 phase-to-impurity ratio is 66:34.

onmental influences, with time a typical floor not only consists of the original phases but also of degradation products, of which the most important is a magnesium chlorocarbonate phase (chlorartinite). The formation of the latter can be explained by the degradation of the F5 phase to the F3 phase, according to $Mg_3(OH)_5Cl{\cdot}4H_2O$ (F5) $\Rightarrow$ $Mg_2(OH)_3Cl{\cdot}4H_2O$ (F3) + $Mg(OH)_2$ and consecutively by carbon dioxide from the air to chlorartinite $Mg_2(OH)_3Cl{\cdot}4H_2O$ (F3) + CO_2 $\Rightarrow$ $Mg_2CO_3(OH)Cl{\cdot}2H_2O$ + $3H_2O$. The massive occurrence of chlorartinite serves as an indicator of problematic floors. We recently succeeded in solving the crystal structure of chlorartinite (Sugimoto *et al.*, 2006). The zeolite-like channel structure of chlorartinite acts as a buffer for excess $MgCl_2$ in solution, making it very vulnerable to changes in temperature or humidity (Sugimoto, Dinnebier & Schlecht, 2007). Excess $MgCl_2$ in solution leads to the occurrence of $MgCl_2{\cdot}6H_2O$ (bischofite) or its lower hydrates $MgCl_2{\cdot}4H_2O$, $MgCl_2{\cdot}2H_2O$ or $MgCl_2{\cdot}H_2O$. The crystal structures of the latter three have recently been determined from synchrotron powder diffraction data, depending on temperature (Sugimoto, Dinnebier & Hanson, 2007).

In a typical Sorel cement *ca* 2/3 of the cement consists of inert filler materials, with quartz sand as the dominant phase. Depending on the impurities of the binder and filler and on the pigments used, a whole list of minerals (most of them having known crystal structures) are found, *e.g.* calcite, aragonite, hematite, magnesite, feldspar, talcum, muscovite, *etc*. It is known that the binder of a perfect floor, prepared with high-quality materials (*e.g.* high magnesium oxide reactivity) in equilibrium conditions, consists exclusively of the F5 phase (Matković *et al.*, 1977). Once the F5 phase is transformed to the F3 phase and chlorartinite during degradation, the mechanical strength decreases considerably (de Castellar *et al.*, 1996).

As already pointed out (Shively, 1916), the use of inferior components and/or excess water leads to various problems like the occurrence of cracks in expanding or contracting floors, decoloring, crumbling floors *etc.* To investigate these phenomena, it is crucial to know the mineralogical composition of these floors quantitatively. Although wet chemical analysis provides some insight into the distribution of elements, the mineralogical composition is much more meaningful. In order to control the production or to evaluate structural damage in the construction business, a full quantitative phase analysis (QPA) using the Rietveld method is necessary, for which knowledge of the crystal structures of the components is essential.

The only major constituent of unknown crystal structure was the F5 phase. Since single crystals of a suitable quality for single-crystal analysis were difficult to grow, we decided to investigate its crystal structure from high-resolution laboratory powder diffraction data. Using this structure in a practical application, a full quantitative phase analysis of two problematic unintentionally bleached magnesia floor was performed, revealing possible causes for the technical failure.

2. Experimental

2.1. Synthesis

To produce a sample of the F5 phase with good crystallinity, but as close as possible to the industrial process, different amounts (555–972 g) of magnesium oxide (H100, van Mannekus, Netherlands) of natural origin were mixed at room temperature with 625 ml of an aqueous solution of magnesium chloride (equivalent to 24° Bé of a $MgCl_2{\cdot}6H_2O$:H_2O weight ratio of 1:1) and kept for 1 week until crystallization was completed. Depending on the molar ratio of MgO:$MgCl_2$, different amounts of the F5 phase with different crystallinity were formed. The sample with the best crystallinity, as checked by high-resolution laboratory powder diffraction, corresponded to a MgO:$MgCl_2$ ratio of $\sim$ 7:1 and was used for structural analysis.

Table 1
Crystallographic data of $Mg_3(OH)_5Cl{\cdot}4H_2O$ (F5 phase).

Crystal data	
Chemical formula	$H_{13}ClMg_3O_9$
M_r	265.46
Cell setting, space group	Monoclinic, *P*2/*m*
Temperature (K)	295
a, *b*, *c* (Å)	9.6412 (5), 3.1506 (2), 8.3035 (5)
β (°)	113.986 (6)
V (Å^3)	230.44 (3)
Z	1
D_x (Mg m^{-3})	1.913
Radiation type	Cu $K\alpha_1$
Specimen form, colour	Particle morphology, white
Data collection	
Diffractometer	Bruker D8 advance diffractometer
Data collection method	Specimen mounting: glass capillary; mode: transmission; scan method: continuous
Refinement	
Refinement on	Full-matrix least-squares on F^2
R_{exp}†	0.0185
R_p†	0.0419
R_{wp}†	0.0598
R_{Bragg}†	0.0120
Wavelength of incident radiation (Å)	1.54059
Profile function profiles in *TOPAS*	Fundamental parameters convolution-based
Starting angle (° 2θ)	5.0000
Final angle (° 2θ)	79.993
Step width (° 2θ)	0.0172
Time/step (s)	20.64
No. of reflections	186
No. of parameters	16
H-atom treatment	H-atom parameters not defined
Weighting scheme	Based on measured s.u.s
$(\Delta/\sigma)_{max}$	< 0.0001

† R_{exp}, R_p, R_{wp} and R_{Bragg} as defined in *TOPAS* (Bruker AXS, 2006).

2.2. Powder diffraction

A high-resolution X-ray powder diffraction pattern of a sample with F5 as the major phase was recorded at room temperature on a laboratory powder diffractometer [D-8, Bruker, Cu $K\alpha_1$ radiation from a primary Ge(111)-Johanson-type monochromator; VÅNTEC-1 position-sensitve detector] in Debye–Scherrer geometry with the sample sealed in a borosilicate glass capillary of 0.5 mm diameter (Hilgenberg glass No. 50). Data were taken in steps of 0.0172° 2Θ from 5.0 to 80.0° 2Θ for 0.05° min^{-1} (Fig. 1). The sample was spun during measurement for better particle statistics.

A qualitative phase analysis using the powder diffraction file (PDF) database and the program *MATCH!* 1.4b (Brandenburg & Putz, 2006) revealed the presence of unreacted magnesium oxide (periclase), and small amounts of brucite, forsterite and quartz as natural impurities of the magnesium oxide. For indexing, structure determination and refinement the program *TOPAS*3.0 (Bruker AXS, 2006) was used. Indexing was performed by iterative use of singular value decomposition (LSI; Coelho, 2003), leading to a primitive monoclinic unit cell with lattice parameters given in Table 1. The lattice parameters matched those of the reduced cell, as given in PDF database #7-420 (de Wolff, 1949). The number of formula units per unit cell could be determined to be $Z = 1$ from volume increments. The extinctions found in the powder patterns indicated either *P*2, *Pm* or *P*2/*m* as possible space groups, of which *P*2/*m* could later be confirmed by Rietveld refinement (Rietveld, 1969). The peak profiles and precise lattice parameters were determined by a LeBail fit (Le Bail *et al.*, 1988) using the fundamental parameter approach of *TOPAS* (Cheary *et al.*, 2004). All the impurity phases were Rietveld refined using starting values from the ICSD database (Schmahl *et al.*, 1964: CSD #60492 for periclase, Greaves & Thomas, 1986: CSD #34401 for brucite, Kirfel *et al.*, 2005: CSD #171572 for forsterite, and Brill *et al.*, 1939: CSD #29122 for quartz). Structure determination of the F5 phase was performed by the global optimization method of simulated annealing (SA), as implemented in *TOPAS* (Coelho, 2000). At the beginning, an ideal MgO_6 octahedron built by the rigid-body editor in *TOPAS*, an Mg atom and a Cl atom were introduced in the SA process. During the SA runs, all other phases and the peak-profile parameters were kept fixed. The site occupancy of the possible special positions was automatically taken care of by introducing a merging radius of 0.6 Å. After 10 min a reasonable structural model was found, which was immediately subjected to a Rietveld refinement. Identical structures were obtained for space groups *P*2 and *P*2/*m*. The occupancy of the free chlorides refined to 75%, suggesting either every fourth chloride statistically being empty or (more likely) a mixed occupancy of 50% H_2O and 50% Cl^-. The possibility of an ordered variant with chlorides and water molecules on separate sites in the space group *Pm* was checked by Rietveld refinement, but led to considerably poorer agreement factors. We therefore decided to continue with the disordered model in *P*2/*m*. A quantitative analysis of all phases, which was included in the Rietveld refinement (Fig. 1), led to the agreement factors (*R* values) listed in Table 1. Thus, the F5 phase-to-impurity ratio is 66:34. Atomic coordinates, bond lengths and bond angles are presented in the supplemental material.[1] The crystallographic data of the F5 phase have been deposited at FIZ Karlsruhe under CSD #417913.

3. Results and discussion

3.1. Structure description

The crystal structure of $Mg_3(OH)_5Cl{\cdot}4H_2O$ (F5 phase) consists of infinite triple chains of almost regular MgO_6 octahedra running along the *b* axis and intercalated disordered chlorides and water molecules (or hydroxides; Figs. 2*a* and *b*). The octahedron in the middle of the triple chain shares six out of 12 edges and all six corners with four neighbouring octahedra. The outer octahedra share four edges, three corners with two, and two corners with one neighbouring octahedron. Thus, the distinction between OH^- and OH_2 can be made by applying Pauling's rules, as has been already

[1] Supplementary data for this paper are available from the IUCr electronic archives (Reference: KD5015). Services for accessing these data are described at the back of the journal.

suggested by de Wolff and Walter-Lévy (1953) for the related F3 phase. The protruding corners of the octahedron must be occupied by H_2O, while the corners shared by three octahedra can only be occupied by OH^-. The corners shared by just two octahedra can be occupied by H_2O or OH^-. For reasons of charge equalization, two alternatives remain. First, if the channels are occupied by disordered chlorides and hydroxides, a hydroxide sits statistically on every fourth corner shared by two octahedra. Second, if the channels (similar to those in the F3 phase) are occupied by chlorides and water molecules, corners shared by two octahedra are occupied alternately by water molecules and hydroxides. The triple chains are thus formed by one $Mg(OH)_6$ and two $Mg(OH)_3(OH_2)_3$ or $Mg(OH)_4(OH_2)_2$ octahedra.

In the crystal structure of the triclinic F3 phase (de Wolff & Walter-Lévy, 1953), chains of MgO_6 octahedra run along the *b* axis, parallel to chains of chlorides and water molecules (Fig. 3). In contrast to the F5 phase, double chains of $Mg(OH)_4(OH_2)_2$ octahedra are formed and the chains of intercalating Cl atoms and water molecules are alternating and thus are ordered.

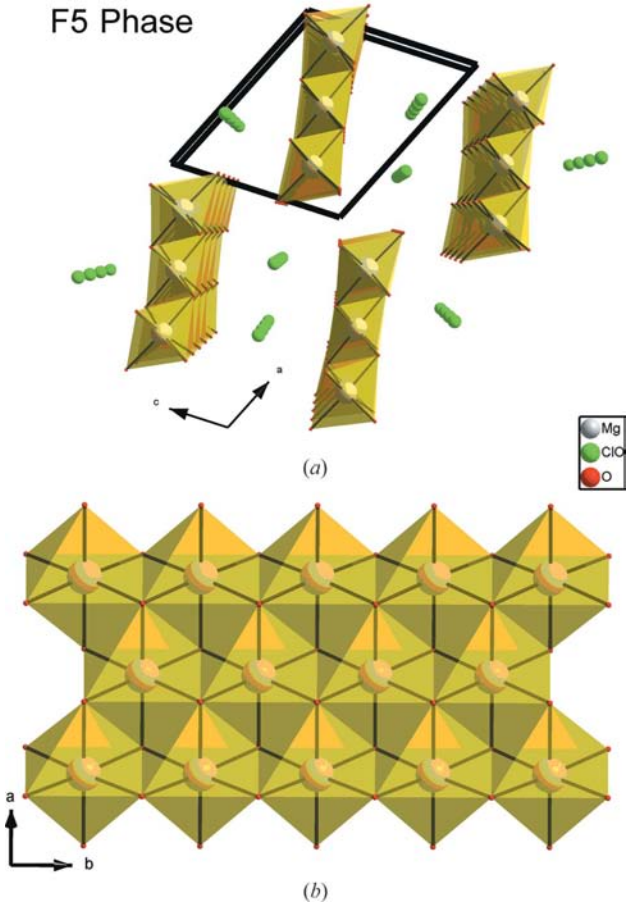

Figure 2
(*a*) Perspective view of the crystal structure of $Mg_3(OH)_5Cl{\cdot}4H_2O$ (F5 phase) at T = 295 K in a central projection (camera distance of 35 cm) down the crystallographic *b* axis. Oxygen positions are in red, chloride positions are in light green and magnesium positions are in yellow. Semi-transparent MgO_6 octahedra are drawn. (*b*) Triple chain with one $Mg(OH)_6$ and two $Mg(OH)_4(OH_2)_2$ octahedra (semi-transparent view) as building units in the crystal structure of $Mg_3(OH)_5Cl{\cdot}4H_2O$ (F5 phase) at T = 295 K along the crystallographic *b* axis. Oxygen positions are in red and magnesium positions are in yellow. H atoms are not shown.

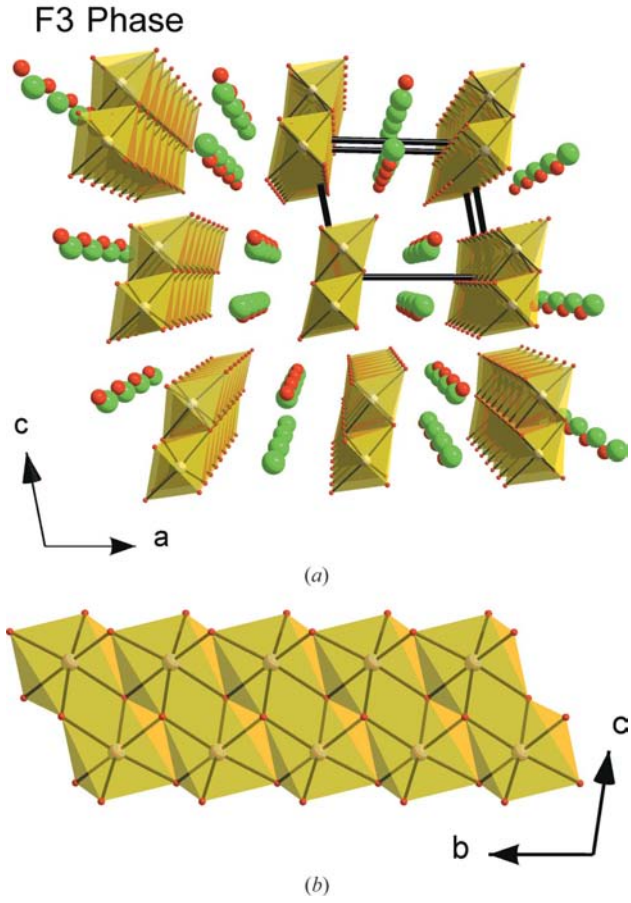

Figure 3
(*a*) Perspective view of the crystal structure of $Mg_2(OH)_3Cl{\cdot}4H_2O$ (F3 phase) at T = 295 K in a central projection (camera distance of 35 cm) down the crystallographic *b* axis. Oxygen positions are in red, chloride positions are in light green and magnesium positions are in yellow. Semi-transparent MgO_6 octahedra are drawn. (*b*) Double chain with two $Mg(OH)_4(OH_2)_2$ octahedra (semi-transparent view) as building units in the crystal structure of $Mg_2(OH)_3Cl{\cdot}4H_2O$ (F3 phase) at T = 295 K along the crystallographic *b* axis. Oxygen positions are in red and magnesium position are in yellow. H atoms are not shown.

Figure 4
Core drill samples of a yellow magnesia floor from southern Germany. The yellow colour was achieved by mixing iron oxides into the MgO powder. Left: correctly colored sample; right: bleached sample.

The Mg—O bond lengths of 1.96—2.14 Å for the F5 phase are within the expected range and are comparable to those of the related F3 phase (de Wolff & Walter-Lévy, 1953). The shortest contact distances between the Cl atom and the corners of the $Mg(OH)_4(OH_2)_2$ octahedron are 3.04 Å for Cl1···O4 (x, y, $-1+z$) and 3.28 Å for Cl1···O1, allowing the formation of hydrogen bonds, which results in an increase in stabilization of the crystal structure.

3.2. Quantitative phase analysis

With the structure determination of the F5 phase, the crystal structures of all significant binder phases occurring during or after the formation process of Sorel cements are finally known. These phases are: periclase (Bragg, 1920), brucite (Aminoff, 1921), bischofite (Andress & Gundermann, 1934) and its lower hydrates (Sugimoto, Dinnebier & Hanson, 2007), F3 (de Wolff & Walter-Lévy, 1953), F5 (this work), and chlorartinite (Sugimoto *et al.*, 2006). The mineralogical composition of a Sorel cement can now be determined routinely to a high precision using quantitative phase analysis (QPA) by the Rietveld method. Such an analysis can be used to determine the quality of a magnesia floor and to find out the causes of cracks and decoloring effects caused by late crystallization. For a practical test, two magnesia floors (colored with iron oxide pigments) which were exhibiting unwanted bleached spots were selected. Floor (1): Industrial quality magnesia floor MA C50 in anthracite color, installed in a production plant in southern Germany in 2006. Light grey spots of diameter 10–200 cm occurred 4–8 weeks after installation of the floor without any obvious cause. Floor (2) industrial quality magnesia floor MA C50 in a yellow color, installed in 2007 in a showroom of a manufacturer of magnesia screeds. White spots appeared within a few minutes after pouring and quickly removing the water on the floor for cleaning purposes (Fig. 4).

For the analysis of the magnesia floors, four samples were taken by carefully filing off several milligrams of the material from drilling cores using a diamond file: sample (1*a*) interior of floor (1); sample (1*b*) decolored surface of floor (1); sample (2*a*) correctly colored surface of floor (2); sample (2*b*) decolored surface of floor (2). The powder patterns were measured using a Bruker D8 high-resolution laboratory powder diffractometers in Debye–Scherrer mode [samples (1*a*) and (1*b*)] or in Bragg–Bren-

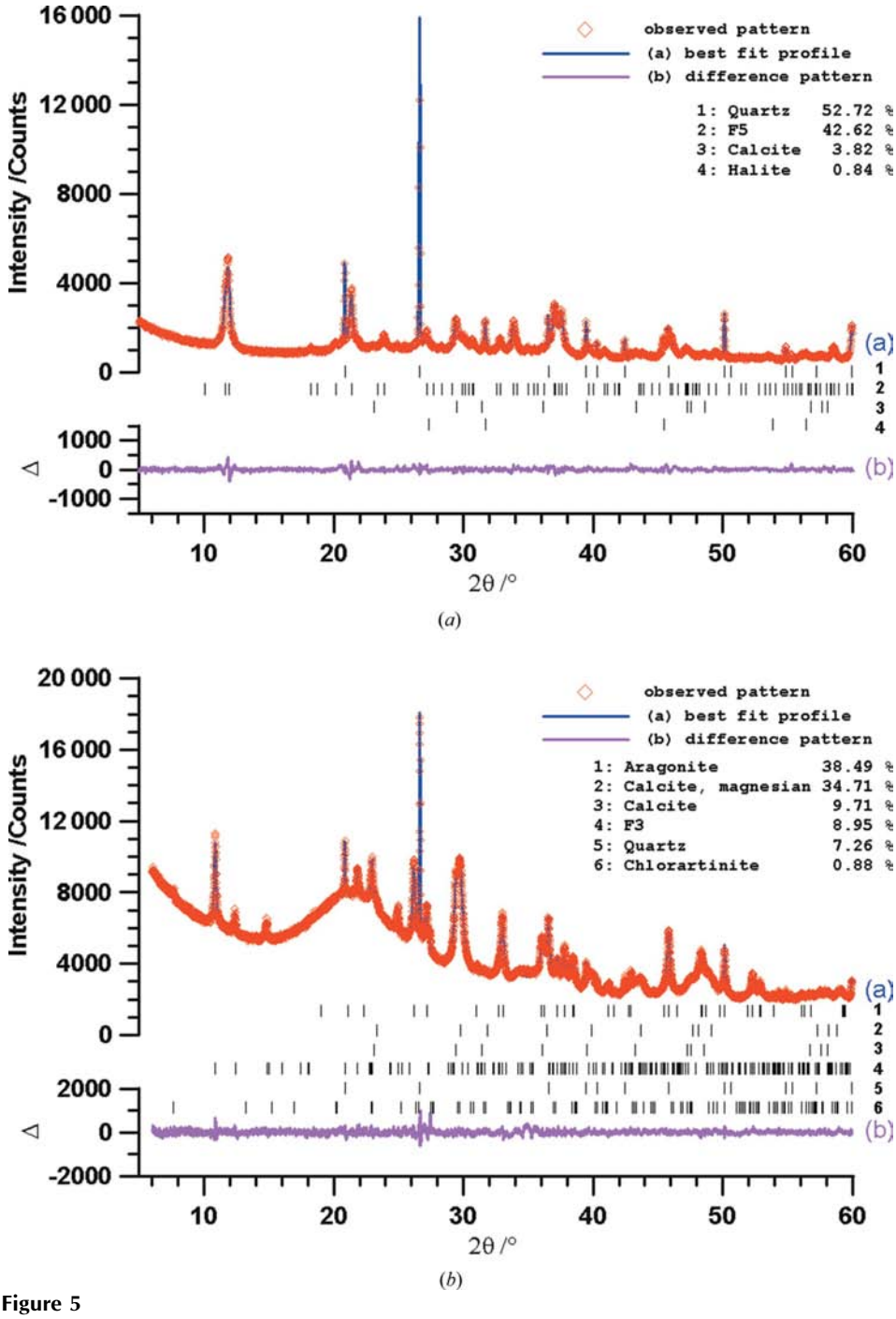

Figure 5
(*a*) Rietveld plot of a sample taken from the interior of a black magnesia floor at $T = 295$ K from southern Germany, containing quartz, F5-phase calcite and traces of rock salt. (*b*) Rietveld plot of a sample taken from the surface of the floor of (*a*) at $T = 295$ K, containing quartz, F5-phase calcite, magnesium calcite, aragonite, F3 phase and traces of chlorartinite.

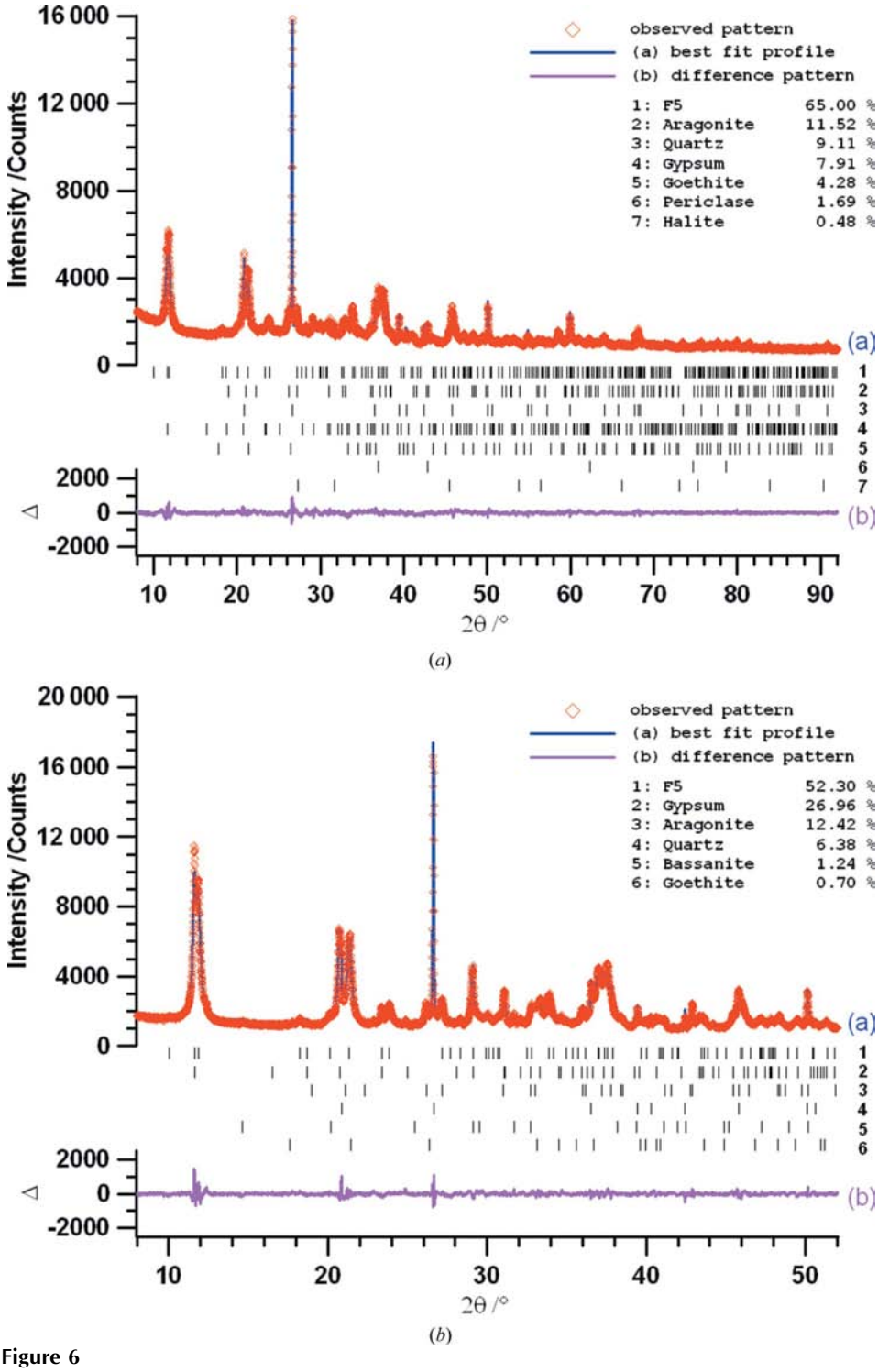

Figure 6
(*a*) Rietveld plot of a sample taken from the surface of the correctly colored yellow magnesia floor of Fig. 4 (left) at $T = 295$ K, containing quartz, F5 phase, aragonite, gypsum, goethite, and traces of periclase and rock salt. (*b*) Rietveld plot of a sample taken from the surface of the bleached yellow magnesia floor of Fig. 4(*b*) (right) at $T = 295$ K, containing quartz, F5 phase, aragonite, gypsum, and traces of bassanite and goethite.

tano geometry [samples (2*a*) and (2*b*)]. For the QPA by the Rietveld method, the *TOPAS* software was used.

In the case of sample (1), there is a huge difference between the mineralogical compositions of the surface (Fig. 5*a*) and of the interior of the floor (Fig. 5*b*). While the interior shows the expected composition of an equilibrated magnesia floor with F5 as the only binding phase, the surface is characterized by a thin layer of calcium carbonate in different crystalline forms and the decomposition products of the F5 phase, namely the F3 phase and chlorartinite. This can be taken as evidence that the floor was correctly laid, but the surface was quite likely exposed to excessive water during the curing process of the floor. The F5 phase transformed to F3 and subsequently to chlorartinite while calcium ions[2] were transported to the surface and reacted with CO_2 from air to form different polymorphs of calcium carbonate.

The situation for sample (2) is entirely different, pointing to a problem with the starting materials. The samples from the correctly colored and the decolored surface both reveal a substantial amount of gypsum [8% for (2*a*) and 28% for (2*b*)]. It can be assumed that gypsum as an undesired component was already present in the raw material before the floor was laid. Owing to its good solubility, the concentration of gypsum in water is enriched in the liquid water during the drying process and brought to the surface by capillary action. When the water evaporates, a thin film of gypsum (and bassanite) is deposited on the surface of the floor. Depending on the local concentration, severe bleaching can occur (Fig. 4).

From Figs. 5 and 6 it is evident that the peak overlap between the F5 phase and the components responsible for damage by bleaching is severe, making the knowledge of the crystal structure of the F5 phase a prerequisite for a successful QPA.

Financial support by the Bundesministerium für Bildung und Forschung (BMBF), the Rigaku Corporation, and the

[2] The amount of reactive calcium within natural magnesium oxide and magnesium chloride varies for different batches and is usually quantitatively analyzed by the manufacturers of the Sorel cement.

Fonds der Chemischen Industrie (FCI) is gratefully acknowledged.

References

Aminoff, G. (1921). *Z. Kristallogr. Kristallgeom. Kristallphys. Kristallchem.* **56**, 505–509.

Andress, K. R. & Gundermann, J. (1934). *Z. Kristallogr. Kristallgeom. Kristallphys. Kristallchem.* **87**, 345–369.

Bilinski, H., Matkovic, B., Mazuranic, C. & Zunic, T. B. (1984). *J. Am. Ceram. Soc.* **67**, 266–269.

Bragg, W. L. (1920). *Nature*, **105**, 646.

Brandenburg, K. & Putz, H. (2006). *MATCH!*, Version 1.4b. Crystal Impact GbR, Bonn, Germany.

Brill, R., Hermann, C. & Peters, C. (1939). *Naturwissenschaften*, **27**, 676–677.

Bruker AXS (2006). *TOPAS*. Bruker AXS Inc., Karlsruhe, Germany.

Castellar, M. D. de, Lorente, J. C., Traveria, A. & Tura, J. M. (1996). *Cem. Concr. Res.* **26**, 1199–1202.

Cheary, R. W., Coelho, A. A. & Cline, J. P. (2004). *J. Res. Natl. Inst. Stand. Technol.* **109**, 1–25.

Coelho, A. A. (2000). *J. Appl. Cryst.* **33**, 899–908.

Coelho, A. A. (2003). *J. Appl. Cryst.* **36**, 86–95.

Greaves, C. & Thomas, M. A. (1986). *Acta Cryst.* B**42**, 51–55.

Kirfel, A., Lippmann, T., Blaha, P., Schwarz, K., Cox, D. F., Rosso, K. M. & Gibbs, G. V. (2005). *Phys. Chem. Miner.* **32**, 301–313.

Le Bail, A., Duroy, H. & Fourquet, J. L. (1988). *Mater. Res. Bull.* **23**, 447–452.

Matković, B., Popović, S., Rogić, V. & Žunić, T. (1977). *J. Am. Ceram. Soc.* **60**, 504–507.

Rietveld, H. M. (1969). *J. Appl. Cryst.* **2**, 65–71.

Schmahl, N. G., Barthel, J. & Eikerling, G. F. (1964). *Z. Anorg. Allg. Chem.* **332**, 230–237.

Shively, R. R. (1916). *J. Indust. Eng. Chem.* **8**, 679–682.

Sorel, S. (1867). *Cem. C. R.* **65**, 102–104.

Sugimoto, K., Dinnebier, R. E. & Schlecht, T. (2006). *J. Appl. Cryst.* **39**, 739–744.

Sugimoto, K., Dinnebier, R. E. & Schlecht, T. (2007). *Powder Diffr.* **22**, 64–67.

Sugimoto, K., Dinnebier, R. E. & Hanson, J. C. (2007). *Acta Cryst.* B**63**, 235–242.

Wolff, P. M. de (1949). Technisch Physische Dienst, Delft, Netherlands, ICDD Grant-in-Aid.

Wolff, P. M. de & Walter-Lévy, L. (1953). *Acta Cryst.* **6**, 40–44.